Self-Assembling Peptide-Polymer Nano-Objects via Polymerization-Induced Self-Assembly

Tuyen T. P. Dao, Lubomir Vezenkov, Gilles Subra, Muriel Amblard, Martin In, Jean-François Le Meins, Florian Aubrit, Mohammad-Amin Moradi, Vincent Ladmiral, M. Semsarilar

▶ **To cite this version:**

Tuyen T. P. Dao, Lubomir Vezenkov, Gilles Subra, Muriel Amblard, Martin In, et al.. Self-Assembling Peptide-Polymer Nano-Objects via Polymerization-Induced Self-Assembly. Macromolecules, 2020, 53 (16), pp.7034-7043. 10.1021/acs.macromol.0c01260 . hal-02915614

HAL Id: hal-02915614
https://hal.science/hal-02915614

Submitted on 11 Dec 2020

HAL is a multi-disciplinary open access archive for the deposit and dissemination of scientific research documents, whether they are published or not. The documents may come from teaching and research institutions in France or abroad, or from public or private research centers.

L'archive ouverte pluridisciplinaire **HAL**, est destinée au dépôt et à la diffusion de documents scientifiques de niveau recherche, publiés ou non, émanant des établissements d'enseignement et de recherche français ou étrangers, des laboratoires publics ou privés.

Self-assembling Peptide – Polymer Nano-Objects *via* Polymerization-Induced Self-Assembly

*T. P. Tuyen Dao[a,b,c], Lubomir Vezenkov[c], Gilles Subra[c], Muriel Amblard[c], Martin In[d], Jean-François Le Meins[e], Florian Aubrit[e], Mohammad-Amin Moradi[f], Vincent Ladmiral[b], Mona Semsarilar[a]**

a: Institut Européen des Membranes, IEM, Univ Montpellier, CNRS, ENSCM, Montpellier, France.

b: Institut Charles Gerhardt Montpellier, ICGM, Univ Montpellier, CNRS, ENSCM, Montpellier, France.

c: Institut des Biomolécules Max Mousseron, IBMM, Univ Montpellier, CNRS, ENSCM, Montpellier, France.

d: Laboratoire Charles Coulomb, L2C, Univ Montpellier, CNRS, Montpellier, France.

e: Laboratoire de Chimie des Polymères Organiques, LCPO UMR 5629, Université Bordeaux, CNRS, Pessac, France.

f: Institute for Complex Molecular Systems, Eindhoven University of Technology, Eindhoven, The Netherlands.

KEYWORDS: PISA, Polymerization-induced self-assembly, Self-assembling peptide, peptide-polymer nano-objects

ABSTRACT: Self-assembling peptides (SAP) have been extensively studied for their ability to form nanoscale ordered structures driven by non-covalent molecular interactions. Meanwhile, polymerization-induced self-assembly (PISA) has been exploited as a facile and efficient way to produce various amphiphilic block copolymer nano-objects, whose self-assembly was governed predominantly by the interactions of the different blocks with the polymerization medium. In this work, we combined PISA with SAP to prepare novel peptide-polymer hybrid nano-objects, thus harnessing the advantages of PISA and the self-assembling driving force of SAP. A tripeptide methacrylamide derivative (MAm-Gly-Phe-Phe-NH_2, denoted MAm-GFF where MAm means methacrylamide) was copolymerized with glycerol monomethacrylate (GMA) to produce P(GMA_{65}-*stat*-$(MAm\text{-}GFF)_7$) macro-chain transfer agent (macro-CTA) by Reversible addition-fragmentation chain transfer (RAFT) polymerization in DMF. This peptide-based macro-CTA was then successfully chain-extended with poly(2-hydroxypropyl methacrylate) (PHPMA) by aqueous dispersion PISA, forming P(GMA_{65}-*stat*-$(MAm\text{-}GFF)_7$)-*b*-$PHPMA_{28}$ self-assembled objects. Fibrous structures were observed by TEM and Cryo-TEM in agreement with DDLS, SLS and SAXS experiments that also revealed long anisotropic morphologies. Such structures have not been reported previously for PISA-prepared nano-objects. This confirms the decisive influence of the GFF SAP on the self-assembly. In addition, annealing the PISA suspension at different temperatures led to a significant size decrease of the self-assembled objects and to a morphological transition caused by the thermo-sensitivity of both the core-forming PHPMA block and the stabilizing P(GMA-*stat*-(MAm-GFF)) block.

INTRODUCTION

Polymerization-induced self-assembly (PISA) is a way to produce block copolymer nano-objects, in which the self-assembly is induced during the formation of the block copolymer. In PISA, a solvent–soluble first polymer is chain extended with a second polymer generally using a reversible deactivation radical polymerization (RDRP) technique.[1-7] The polymerization solvent is chosen to be selective of the

first block so that the growing second block becomes insoluble as the polymerization progresses, thus inducing the self-assembly in-situ. First reported in 2002,[8] although not called PISA then, this simple synthetic method gained momentum in the last few years[9] for its ability to produce well-defined polymer nano-objects at high concentration and with high reproducibility. PISA has been demonstrated to work well under dispersion[10-14] or emulsion polymerization[15-18] both in polar solvents (water, alcohols, …)[19-25] or non-polar solvents (alkanes, toluene, …).[26-29] Less conventional solvents such as ionic liquids[30] or supercritical CO_2[31-33] were also successfully used for PISA protocols. Although PISA can result in a large variety of morphologies, spheres, worms or vesicles with controlled size and functionality[2, 11, 34-38] are the most common PISA morphologies.

Hybrid peptide-polymers are an important class of materials combining interesting characteristics of their peptide and polymer components. Ideally, these structures should possess the biocompatibility and biofunctionality of peptides as well as the robustness and functional diversity conferred by the polymer chains. They can be prepared by various approaches (i.e. post polymerization grafting, grafting-from or grafting-through)[39-43] resulting in a wide variety of morphologies, functionalities and potential applications. Recently, our group reported the first polypeptide-polymer nanoparticles synthesized *via* PISA.[44] These hybrid particles were composed of a hydrophilic trilysine-containing shell and a PHPMA hydrophobic core. The cationic oligolysine was shown to confer antibacterial properties to the self-assembled structures.

Nano-objects based on peptides self-assembly have also gained attraction, especially for tissue engineering and drug delivery applications[45] due to their biocompatibility, and ease of synthesis and modification to yield bioactivity.[46, 47] Self-assembling peptides (SAP) were used in a bottom-up approach to form a variety of stable supramolecular nanostructures, such as fibers, rods, tubes, nano-vesicles or spheres.[45] Their self-assembly is driven by non-covalent interactions such as hydrogen bonding, π-π stacking, van

der Waals forces or electrostatic interactions.[48] Thus, their organization could be triggered and finely regulated by different parameters such as ionic strength, pH and temperature.

In this context, exploring the combination of PISA and SAP peptide in block copolymer self-assembly appears very interesting. Such systems could be significantly influenced not only by physicochemical parameters such as the solubility and the hydrophobic/hydrophilic balance between the two components of the block copolymers, but also by the specific self-recognition properties of the peptide moieties. Consequently, a methacrylamide (MAm) functionalized tripeptide monomer (MAm-Gly-Phe-Phe-NH_2, denoted MAm-GFF) was synthesized. The GFF motif was chosen for the simple diphenylalanine sequence which has been the most extensively studied SAP reported so far.[49, 50] Depending on conditions, this dipeptide and its numerous derivatives can self-assemble into nanotubes,[51] nanowires,[52] nanovesicles[53] or fibers.[54] Aromatic interactions and hydrogen bonds between diphenylalanine moieties are considered critical for the formation of these distinct nanostructures.[55-57] A glycine residue was used as a spacer between the self-recognition element and the polymerizing unit. MAm-GFF was statistically copolymerized with a hydrophilic monomer (glycerol monomethacrylate, GMA) by Reversible addition-fragmentation chain-transfer (RAFT) polymerization to form the target SAP-containing macromolecular chain transfer agent (macro-CTA). This (MAm-GFF)-containing macro-CTA was chain-extended with poly (2-hydroxypropyl methacrylate) (PHPMA) under aqueous dispersion PISA. GMA and HPMA were chosen since they are highly biocompatible and because the PGMA-*b*-PHPMA PISA system has been thoroughly studied and reported,[12, 34, 58-62] thus it constitutes a very useful benchmark to understand the influence of SAP on the final morphologies. The synthetic approach in this work is illustrated in scheme **1**. Scattering and imaging techniques were used to characterize the resulting nano-objects. Particularly, the change in shape and size of the objects was examined *via* cooling-heating cycles.

Scheme 1. Syntheses of the P(GMA-*stat*-(MAm-GFF)) macro-CTA using RAFT and of P(GMA-*stat*-(MAm-GFF))-*b*-PHPMA block copolymers under PISA conditions.

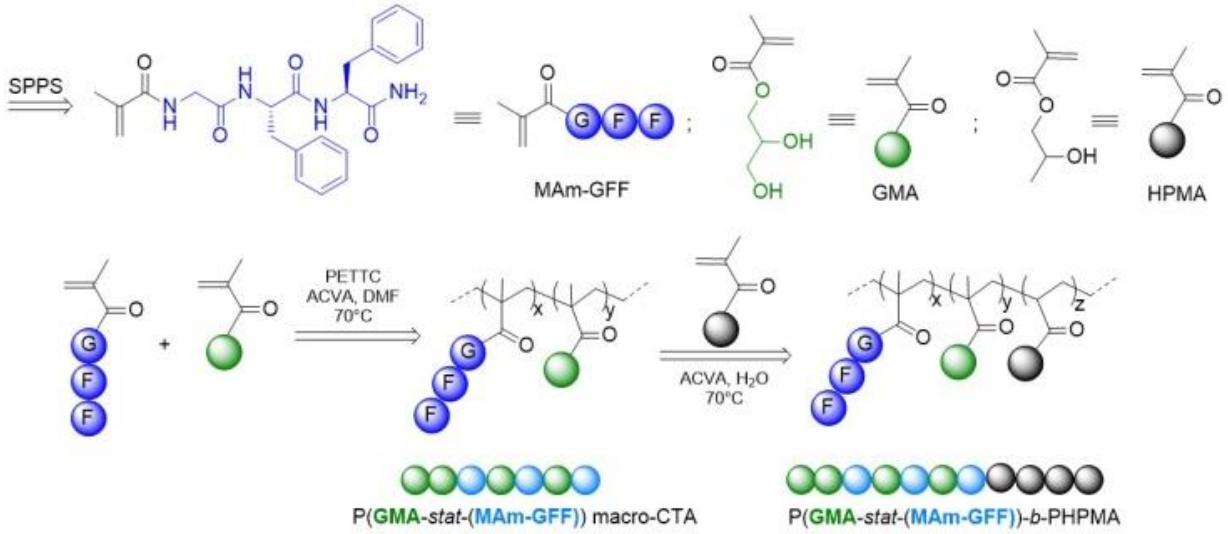

MATERIALS AND METHODS

Materials

Fmoc-amino acid derivatives (Fmoc-Phe-OH, Fmoc-Gly-OH), HATU (1-[Bis(dimethylamino)methylene]-1H-1,2,3-triazolo[4,5-b]pyridinium 3-oxide hexafluorophosphate) and Polystyrene Fmoc Rink Amide resin (100-200 mesh) with a loading of 0.94 mmol/g were purchased from Iris Biotech GmbH. Methacrylic acid, Piperidine, N,N-Diisopropylethylamine (DIEA), Trifluoroacetic acid (TFA), 2-hydroxypropyl methacrylate (HPMA), Glycerol monomethacrylate (GMA), 4,4'-azobis(4-cyanopentanoic acid) (ACVA) and all organic solvents (Dichloromethane (DCM), Acetonitrile (ACN), Dimethylformamide (DMF), Ethanol) were purchased from Sigma-Aldrich. The NMR deuterated solvents (D_2O, DMSO-d6, DMF-d7) were purchased from Eurisotop. The RAFT agent 4-cyano-4-(2-phenylethanesulfanylthiocarbonyl)-sulfanylpentanoic acid (PETTC) was prepared as previously described.[10] All reagents were used as received.

Synthesis of methacrylamide-functionalized peptide monomer (MAm-GFF)

The GFF peptide sequence was prepared using standard Fmoc Solid Phase Peptide Synthesis (SPPS) method[63] with a CEM Liberty® microwave automated peptide synthesizer on a 4 mmol scale (4.26 g resin). DMF was used as solvent, HATU was used as the activating agent in the presence of DIEA and

Piperidine/DMF 20/80 v/v mixture was used as the Fmoc-deprotecting solution. For each amino acid coupling, 35 mL of Fmoc-protected amino acid solution at concentration of 0.4 M in DMF (14 mmol, 3.5 equiv), 14 mL of HATU at concentration 1 M in DMF (14 mmol, 3.5 equiv) and 2.8 mL of DIEA (16 mmol, 4 equiv) was loaded to the microwave reactor. After each coupling, the Fmoc-protecting group was removed with mixture of Piperidine/DMF 20/80 v/v and the resin was washed prior to subsequent coupling. Once target peptide sequence was obtained, the resin was transferred into a reaction vessel and reacted with 35 mL of a mixture containing 1.2 g of methacrylic acid (3.5 equiv), 5.32 g HATU (3.5 equiv), 2.76 mL DIEA (4 equiv) in DMF for 1 h at room temperature. The resin was then washed with DMF (20 mL x 3), then, with DCM (20 mL x 3) and dried by nitrogen purging. The N-terminally methacrylated peptide was cleaved from the resin with a TFA/DCM (1/1) mixture for 2 h at room temperature. The resin was then filtered and concentrated under reduced pressure. The peptide was recovered by precipitation in cold diethyl ether, then taken up in ACN/water 50/50 v/v mixture and freeze-dried. No further purification step was needed. MAm-GFF was obtained as a white solid (1.45 g, 83% yield) and analysed by LC-MS and ^{1}H NMR (Figure **S1**, **S2** Supporting Information). ^{1}H NMR in DMSO δ (ppm): 1.85 (s, 3H, -C*H*$_3$); 2.72 (dd, 2H, -NH-C*H*$_2$-CO); 2.82-3.08 (m, 4H, -CH-C*H*$_2$-Ph); 4.41 (m, 2H, -NH-C*H*CO-CH$_2$-); 5.38 (s, 1H, vinyl); 5.71 (s, 1H, vinyl); 7.10-7.28 (m, 10H, phenyl); 8.08-8.20 (m, 3H, -N*H*-).

Note: All peptides used were enantiomerically pure. They were prepared from a single (L) isomer of each amino acid, with state of the art and well established procedures of solid phase peptide synthesis. In this strategy, the peptides were synthesized stepwise from the C to N terminus using urethane-protected amino acids that avoid any risk of epimerization.

RAFT copolymerization of GMA and MAm-GFF

The general procedure for the synthesis of copolymer P(GMA-*stat*-(MAm-GFF)) macro-CTA is as follows: a round bottom flask equipped with a stirrer bar was charged with GMA (1 g, 6.242 mmol),

MAm-GFF (378 mg, 0.865 mmol), PETTC RAFT agent (32.6 mg, 0.096 mmol), ACVA initiator (2.69 mg, 0.0096 mmol) and DMF. The flask was subsequently sealed with a rubber septum, the reaction mixture was degassed by bubbling nitrogen for 30 min and the flask was immersed in a preheated oil bath at 70°C. The reaction was conducted under stirring for 24h. Then the copolymerization was quenched by opening the reaction to air and the conversion was determined by ^{1}H NMR. GMA conversion was determined from the proton integral ratios of its residual vinyl signals at 5.65 ppm (1H) or 6.15 ppm (1H) to the signals at 3.5-4.1 (5H) whereas the MAm-GFF conversion was obtained from the comparison of its residual vinyl signals at 5.42 (1H) or 5.85 (1H) to the phenyl group at 7.2-7.4 (10H). The reaction solution was diluted in DMF and precipitated in cold THF. The yellow precipitate was then re-dispersed in water and freeze-dried. DMF GPC analysis of final product indicated M_n = 18,290 g/mol with M_w/M_n = 1.32 (Figure **6**) while ^{1}H NMR gave the mean DP of PGMA and PMAm-GFF are 65 and 7 respectively (Figure **S3** Supporting Information).

For the copolymerization kinetic study, DMF-d7 was used as solvent. The reaction mixture was deoxygenated in a Schlenk flask then transferred into an NMR tube under nitrogen atmosphere. The ^{1}H NMR spectra were recorded at time t = 0 (just after putting the sample at 70°C in the NMR spectrometer), at 30 min intervals during the first three hours and every hour for the remaining time until the reaction was finished.

PISA *via* RAFT aqueous dispersion polymerization

PISA protocol was performed *via* RAFT aqueous dispersion polymerization of HPMA with P(GMA$_{65}$-*stat*-(MAm-GFF)$_7$) macro-CTA as described below. The purified P(GMA$_{65}$-*stat*-(MAm-GFF)$_7$) macro-CTA (200 mg, 0.0145 mmol), HPMA (58.5 mg, 0.406 mmol) and ACVA initiator (1.0 mg, 0.0036 mmol) were weighed into a 10-mL glass vial containing a stirrer bar. 2.34 mL MilliQ water was then added to get a reaction solution at 10% w/w. The vial was sealed, degassed for 30 minutes and put into an oil bath previously set at 70°C using a stirring hotplate. After 24h, reaction was opened to the air,

cooled down to ambient temperature and aliquots were taken to run ^{1}H NMR, GPC, TEM, Cryo-TEM, DDLS, SLS and SAXS.

Liquid chromatography – mass spectrometry (LC-MS)

LC-MS analyses were performed on Waters Alliance 2695 HPLC system, coupled to a Water Micromass ZQ spectrometer (electrospray ionization mode, ESI+). The peptide monomer MAm-GFF was dissolved in a small amount of DMF and diluted with acetonitrile/water (50/50 v/v) mixture containing 0.1 % TFA. UV detection was performed at 214 nm.

Proton nuclear magnetic resonance spectroscopy (^{1}H NMR)

^{1}H NMR spectra were recorded on a 300 MHz Bruker Avance-300 spectrometer, processed and analyzed with MestReNova 9.0 software.

Gel Permeation Chromatography (GPC)

Polymer molar mass distributions were analysed using a GPC Varian 390-LC system fitted with 2 PL1113-6300 ResiPore 300 x 7.5 columns thermostated at 70°C and connected to a 390LC PL0390-0601 refractive index detector (RI). The mobile phase was DMF containing 0.1% w/w LiBr at a flow rate of 1 mL min^{-1}. The calibration was achieved with near-monodisperse poly(methyl methacrylate) (PMMA) standards ranging from 550 to 1 568 000 g mol^{-1} (EasiVial-Agilent).

Circular Dichroism (CD)

The CD spectra were recorded on a JASCO J-815 Spectropolarimeter. MAm-GFF was dissolved in ethanol (0.02 and 0.04% w/w) and loaded into a 1 mm quartz cuvette. Spectra were obtained from 190-260 nm with 0.1 nm step, 1 nm bandwidth and 100 nm/min for scanning speed.

X-Ray Diffraction (XRD)

XRD was employed on the Philips Xpert Pro Diffractometer with Cu Ka radiation (k = 1.54 Å). The sample was scanned from 5° to 50° with steps of 0.033°.

Light scattering (LS)

The hydrodynamic radii were analyzed by dynamic light scattering at 90° using an Anton Paar Litesizer TM 500. Samples were prepared at 0.1 % w/w by diluting the PISA suspension 100-fold with MilliQ water. The measurements were performed at 25°C or for varied temperature from 20°C to 70°C with 10°C intervals, 30 minutes of equilibration was set at the target temperature prior each measurement.

Depolarized Dynamic Light Scattering (DDLS) measurements were also performed, thanks to the prototype of the Thetis multiangle DDLS setup commercialized by Cordouan Technologies (Pessac, France) consisting of two detector cells located at various angles respectively to the incident laser beam. Each of the cells detected either the polarized or depolarized transmitted beam, through the splitting of this beam by a polarizing cube. The data for characterizing the anisotropy of the particles were then treated following the theoretical model developed with Broersma's equations.[64]

Small angle X-Ray scattering (SAXS)

The SAXS experiments were performed under transmission configuration using an in-house setup at the Laboratory Charles Coulomb (Montpellier, France). A high brightness, low power X-ray tube, coupled with an aspheric multilayer optic (GeniX^{3D} from Xenocs) delivers an ultralow divergent beam (0.5 mrad, λ = 0.15418 nm). Scatterless slits were used to give a clean 0.6 mm beam diameter with a flux of 35 Mphotons per second) on the sample. Samples were contained in lineman tubes of 1 mm external diameter and 0.1 mm thickness. We worked in a transmission configuration and the scattered intensity was measured using a 2D “Pilatus” 300K pixel detector by Dectris (490*600 pixels) with pixel size of 172*172 μm², at a distance of 1.9 m from the sample. Sample SAXS intensity is the average of six scans obtained after an exposition time of 30min/scan that corresponds to 3 hours of data acquisition time. The 2D signal on the plate was translated into I(q) signal using FIT2D. All intensities were corrected for transmission, empty cell and solvent contribution. The measurements were run directly from the concentrated PISA suspension at 10% w/w.

Transmission Electron Microscopy (TEM)

TEM images were acquired using either a JEOL 1200 EXII – 120 kV or a JEOL 1400 P+ - 120 kV. 10 µL of diluted PISA suspension (0.1 % w/w) was deposited onto the grid for 60 s and then blotted with filter paper to remove excess solution. Afterward, the sample-loaded grid was stained with 7 µL of 1 % ammonium molybdate solution for 20 s before this solution wasremoved with filter paper. The grid was allowed to dry for 5 minutes under the fumehood. For the study at 70°C or 5°C, 10% w/w PISA suspension was incubated at the desired temperature during 1 h and diluted to 0.1 % w/w with MilliQ water at the same temperature. Samples were quickly loaded onto the grid using the protocol described above, but in these cases, the grids were prepared in an oven chamber set at 70°C or in a fridge.

Cryogenic Transmission Electron Microscopy (Cryo-TEM)

Cryo-TEM analysis was performed using a CryoTitan (Fisher Scientific Corp) operating at 300 kV and equipped with a field emission gun (FEG). The TEM grids were glow discharged with a Cressington 208 carbon coater. Vitrified samples were prepared from a 3 µL droplet of solution pipetted on the grid inside the VitrobotTM at the highest relative humidity and room temperature. The samples were blotted to remove the excess solution and plunged into liquid ethane by using the automated vitrification robot, VitrobotTM (Mark III, FEI Corp) to achieve an electron transparent sample in amorphous ice around a lacey carbon grid.

RESULTS AND DISCUSSION

Methacrylamide-functionalized peptide monomer MAm-GFF

Standard Fmoc solid phase peptide synthesis were successfully applied to prepare the methacrylamide-functionalized peptide monomer MAm-GFF with a good yield (83%) and high purity, as proved by LC-MS and ^{1}H NMR spectrum shown in Figure **S1** and **S2** Supporting information. MAm-GFF is rather hydrophobic, insoluble in water but could be dispersed in ethanol. DLS analysis the dispersion of MAm-GFF in ethanol at 0.1 % w/w indicated poor solubility shown by the presence of micrometric

self-assembled objects. Representative TEM images of the structures obtained from this dispersion are shown in Figure **1**. These images show bundles of rather monodisperse fibers, 1.50±0.14 μm long and 0.35±0.03 μm wide, with dozen fibers per bundle, each about 40nm in width. X-Ray powder diffraction proved the crystallinity of these fibers (Figure **2**). The sharp distinct peaks of MAm-GFF are consistent with those seen in the X-ray diffractograms of L-phenylalanine-based molecules.[55, 65-68] Furthermore, CD spectroscopy was also employed to extract more information about the self-assembly of MAm-GFF in ethanol. The clear positive signal observed at 222 nm, also observed in previous studies of L-phenylalanine derivatives, was assigned to π-π* transitions resulting from aromatic stacking of the phenylalanine residues.[69] Hence, the self-organization into supramolecular structures of MAm-GFF was attributed to aromatic stacking interactions between FF moieties. In addition, recent experimental and theoretical studies suggested that the self-assembled nanostructures formed from FF-containing molecules are also stabilized *via* H bonding (FF-FF, FF-solvent) and other weak forces such as hydrophobic, electrostatic and Van der Waals interactions between non-polar moieties.[56] In the case of MAm-GFF, H-bonds between the amide groups most likely contribute to the self-assembly.

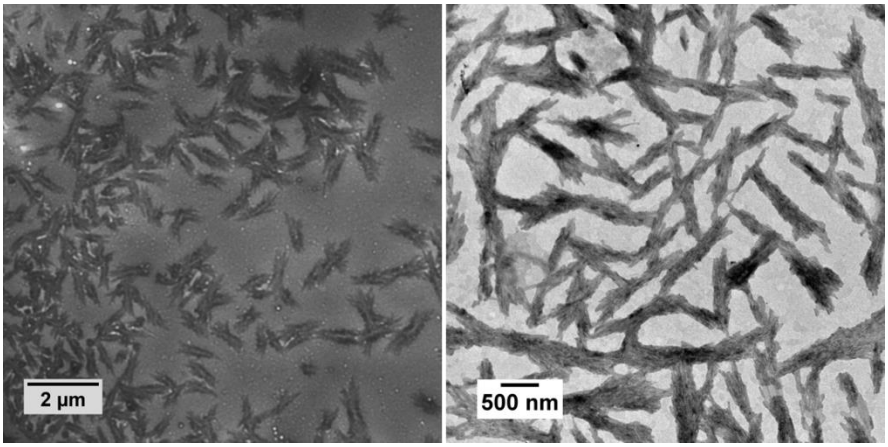

Figure 1. Representative TEM images of structures obtained from MAm-GFF solution in ethanol at 0.1 % w/w.

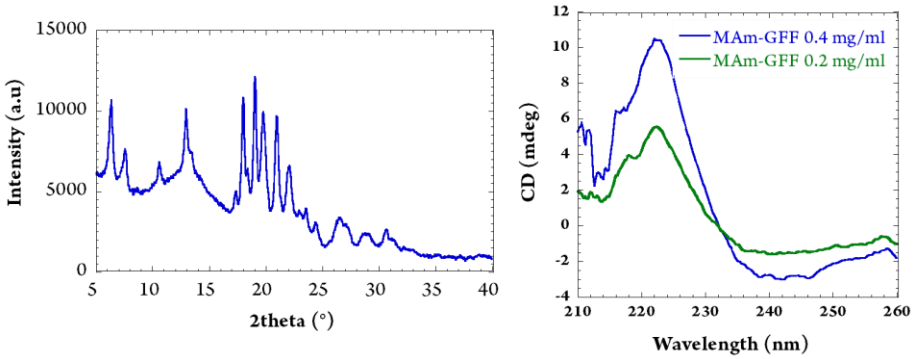

Figure 2. X-ray diffractogram of MAm-GFF powder (left), and CD spectra of MAm-GFF in ethanol at 0.2 and 0.4 mg/mL (right).

P(GMA-*stat*-(MAm-GFF)) macro-CTA

Due to the insolubility of PMAm-GFF in water, PISA protocols in water using such macromolecular chain transfer agent (mCTA) cannot be easily performed. Instead, a more hydrophilic macro-CTAs prepared by copolymerization in DMF of MAm-GFF and glycerol monomethacrylate (GMA, a common monomer in PISA-formulations) was used.[12, 20, 34, 70-73] The monitoring of the conversions of each monomer during the copolymerization by in-situ ^{1}H NMR kinetic study (Figure **3**) shows that MAm-GFF was consumed slightly slower than GMA. GMA was almost completely polymerized after 5h but MAm-GFF conversion only reached 80%. However, both monomers started and stopped copolymerizing at the same time (after about 240 mins). This suggests the formation of a statistical P(GMA-*stat*-(MAm-GFF)) copolymer. The slightly slower rate of polymerization observed for MAm-GFF could be caused by the steric hindrance of the GFF moiety. Using these reaction conditions, a well-defined P(GMA$_{65}$-*stat*-(MAm-GFF)$_7$) copolymer was prepared (M_n = 18,290, Đ = 1.32). This copolymer was easily dispersed in water at 10 % w/w.

DLS and TEM analyses were performed to investigate the assembled-state of this MAm-GFF-containing macro-CTA. The copolymer was dispersed in MilliQ water at a concentration of 0.1 % w/w and stirred gently overnight. TEM images of this dispersion, shown in Figure **4**, revealed the formation of bundles of fibers or ribbons with diameter between 60 and 500 nm. The bundles were about 10 µm and contained a large number of ribbons. Compared to the bundles formed by MAm-GFF (Figure **1**), these copolymer bundles were less aligned and thus formed hyperboloids.

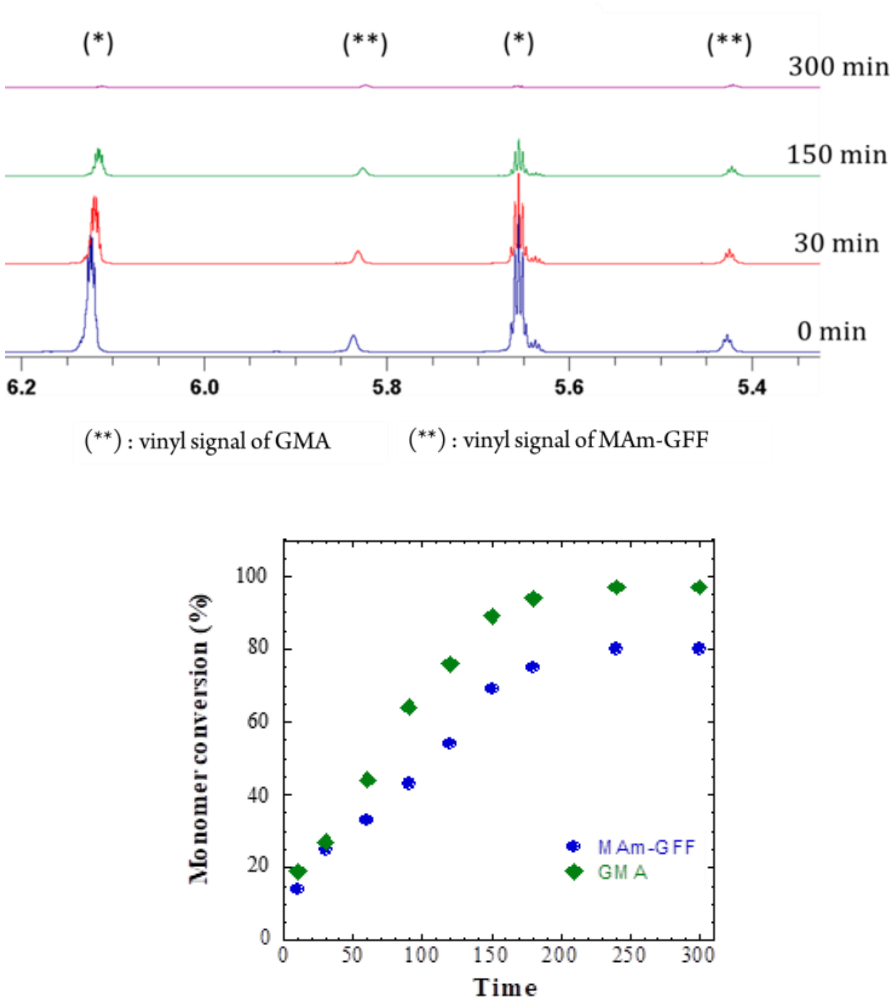

Figure 3. Evolution of monomer conversion with polymerization time for the RAFT statistical copolymerization of GMA and MAm-GFF as studied by ^{1}H NMR spectroscopy. Data points for the GMA and

MAm-GFF are denoted by green lozenges and blue spheres respectively. Reaction conditions: $[GMA]_0$: $[MAm\text{-}GFF]_0$: $[PETTC]_0$: $[ACVA]_0$ = 65: 9: 1: 0.1 in DMF-d7 at 70°C.

The influence of temperature on the self-assembly behavior of the P(GMA_{65}-*stat*-$(MAm\text{-}GFF)_7$) macro-CTA was investigated by DLS and TEM over the 30°C-70°C range. Heating is indeed known to disrupt supramolecular interactions such as H-bonding or pi-stacking. The DLS analyses showed that the size of the self-assembled structures gradually decreased with increasing temperature (Figure **5**). At 30°C, a trimodal size distribution was detected with broad peaks observed at 20 nm, 200 nm and 5 µm. At 40 °C, the smaller peak disappeared and the other distribution narrowed. From 50°C upwards, and at 70°C, only one narrow peak centered at approximately 250 nm was observed. TEM samples prepared at 70°C also confirmed the change in size of the structures, compared to the images taken for samples prepared at ambient temperature (about 30°C). At 70°C, the copolymer still self-assembles into fibrous bundles but of smaller length and diameter. This TEM image also show fuzzier interfaces for the morphologies compared to those imaged at 30 °C, which is consistent with a higher degree of solvation.

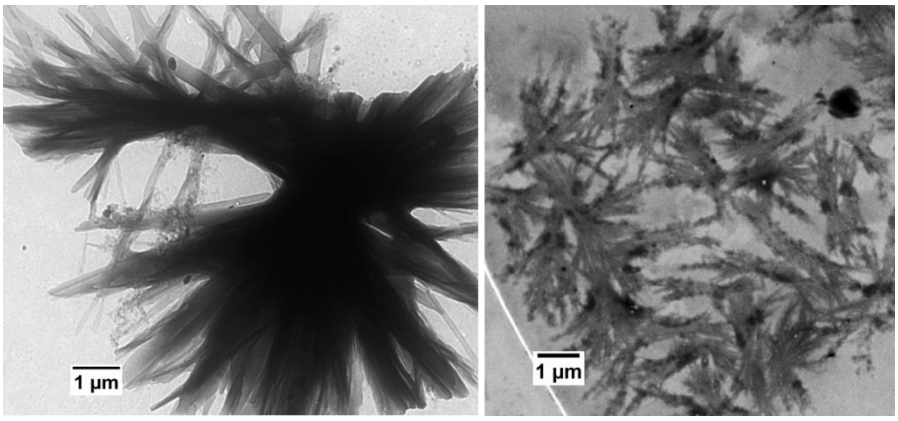

Figure 4. Representative TEM images of P(GMA_{65}-*stat*-$(MAm\text{-}GFF)_7$) macro-CTA in MilliQ water at 0.1% w/w at ambient temperature (about 30°C) (left) and at 70°C (right).

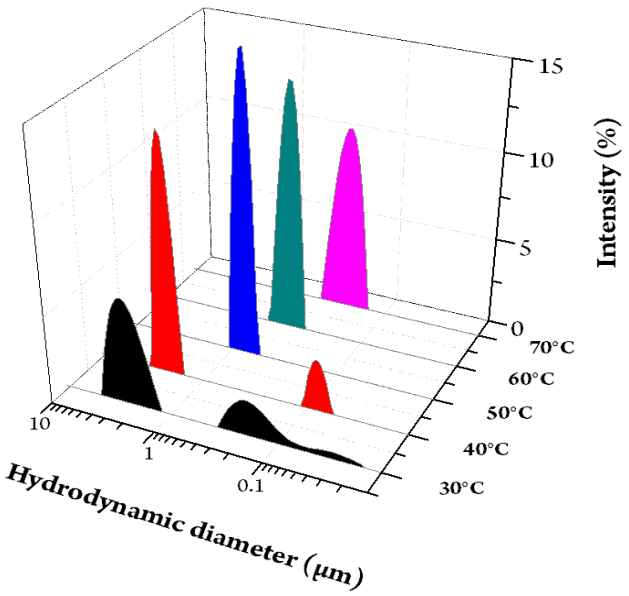

Figure 5. Intensity-average hydrodynamic diameter distribution of P(GMA$_{65}$-*stat*-(MAm-GFF)$_7$) macro-CTA in MilliQ water at 0.1 % w/w over the 30°-70°C range.

To examine the possible influence of HPMA on the structure of the P(GMA$_{65}$-*stat*-(MAm-GFF)$_7$) macro-CTA, a mixture of macro-CTA with HPMA in water at 10 % w/w was prepared and heated overnight at 70 °C. This mixture was then diluted to 0.1 % w/w and analysed by DLS and TEM. As shown in Figure **S4** the TEM images do not show any specific change as compared to the images shown in Figure **4**. In addition, the object size obtained from DLS at 70 °C in presence of HPMA is comparable to the data shown in Figure **5**, suggesting that HPMA does not act as co-solvent for the macro-CTA, as the observed morphology and size were unaffected.

P(GMA-*stat*-(MAm-GFF))-*b*-PHPMA nano-objects *via* PISA

The RAFT aqueous dispersion polymerization of HPMA using the P(GMA$_{65}$-*stat*-(MAm-GFF)$_7$) macro-CTA was conducted at 10 % w/w and yielded well-defined P(GMA$_{65}$-*stat*-MAm-GFF$_7$)-*b*-PHPMA$_{28}$

diblock copolymer self-assembled nanostructures. As in a typical aqueous dispersion polymerization, the reaction mixture became increasingly cloudy, signaling the formation of aggregates. 100% conversion of the HPMA was obtained after 24 h as judged by ^{1}H NMR spectroscopy. Formation of the diblock copolymer *via* chain extension of the macro-CTA with PHPMA was confirmed by SEC as shown in Figure **6** (Đ = 1.32). The resulting diblock copolymer dispersion was stable throughout the polymerization. No sedimentation or creaming was observed and the dispersion remained colloidally stable for six months when stored at 4°C. To

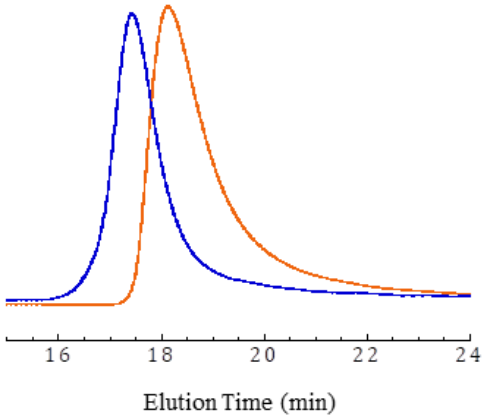

Figure 6. DMF GPC traces (refractive index detector) for the P(GMA$_{65}$-*stat*-(MAm-GFF)$_{7}$) macro-CTA (orange) and the diblock copolymer P(GMA$_{65}$-*stat*-(MAm-GFF)$_{7}$)-*b*-PHPMA$_{28}$ (blue) prepared by RAFT aqueous dispersion polymerization of HPMA at 10 % w/w at 70 °C.

To investigate the morphology of the P(GMA$_{65}$-*stat*-(MAm-GFF)$_{7}$)-*b*-PHPMA$_{28}$ aggregates, TEM analysis was performed on diluted (100-fold) samples. Figure **7** shows that fibrous structures were obtained and that these fibers (80-100 nm) tended to arrange into sharp spherulitic structures. These structures are distinct but related to those observed for the P(GMA$_{65}$-*stat*-(MAm-GFF)$_{7}$) macro-CTA (Figure **4**). However they are completely different from those resulting from the PISA of PGMA-*b*-PHPMA.[12] This clearly underlines the influence of the GFF interactions on the self-assembly process.

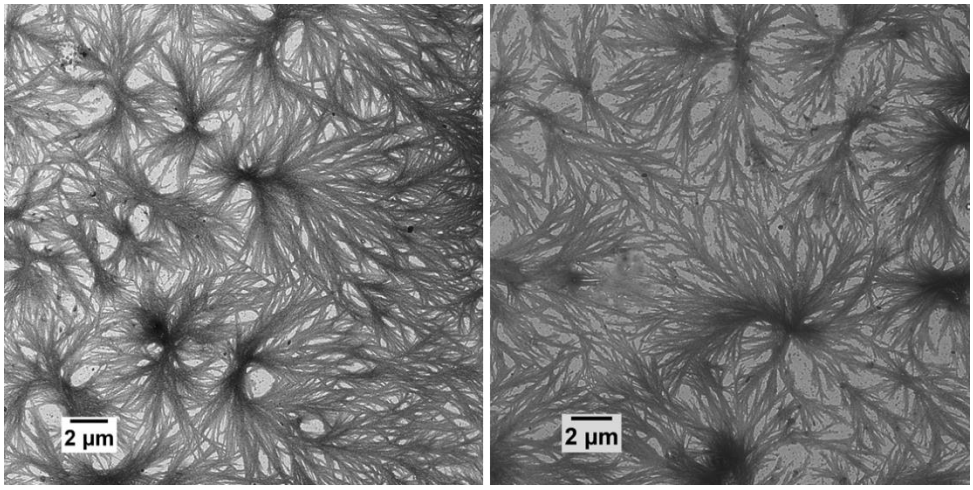

Figure 7. Representative TEM images of the P(GMA_{65}-*stat*-(MAM-$GFF)_7$)-*b*-$PHPMA_{28}$ diblock copolymer morphologies obtained by aqueous dispersion PISA and diluted to 0.1 % w/w at ambient temperature.

To eliminate possible structural changes due to drying and sometimes observed in the case of post-mortem TEM imaging, cryo-TEM and scattering techniques were used to provide further structural information. Figure **8** shows a cryo TEM image of the PISA morphologies obtained from the P(GMA_{65}-*stat*-(MAm-$GFF)_7$)-*b*-$PHPMA_{28}$ diblock copolymer in water: 1-2 µm long and 50-100 nm wide fiber-like objects. These images demonstrate that these fibers are formed during polymerization and are not artefacts due to sample preparation and drying. The bundles visible in the non-cryogenic TEM, however, are absent from the cryo-TEM images and thus likely result from the drying process during post-mortem TEM grid preparation.

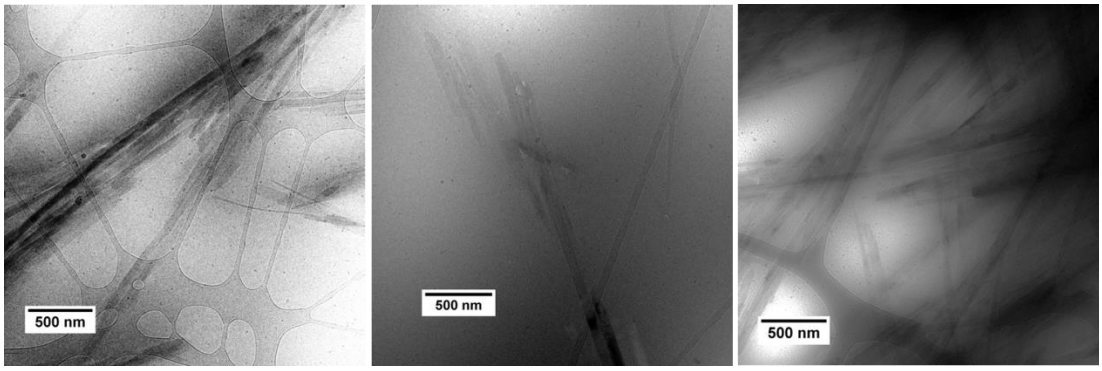

Figure 8. Representative cryo-TEM images of P(GMA_{65}-*stat*-(MAm-$GFF)_7$)-*b*-$PHPMA_{28}$ diblock co-polymers morphologies obtained from aqueous dispersion PISA at 10% w/w.

Traditional DLS analyses where particles are assumed to be spherical are not adequate to examine such anisotropic structures. Hence, simultaneous polarized and depolarized (90°) DLS measurements were performed. In these experiments, two diffusion coefficients are determined: the translational coefficient (D_t) and the rotational coefficient (D_r), thus giving the length (L) and also the width (W) of the objects. The detail of the data analysis procedure can be found in supporting information (Figure **S5- S7**). The average width (w = 250 nm) and the approximate length (200 nm < L < 1 μm) are in agreement with the cryo-TEM images. To further confirm the existence of the fibrous structures in solution, scattering techniques were used. SLS measurement in the q-range 0.005 – 0.035 nm^{-1} was combined with SAXS measurement over the q range 0.005 – 2 nm^{-1}, providing the plot shown in Figure **9**. A plateau of intensity is not obtained at low q, reflecting the presence of large object in the solution compared to the observation window. This plot displays q^{-2} scaling law at low q between 0.005 nm^{-1} and 0.035 nm^{-1} and $q^{-1.5}$ scaling law at intermediate (or high) q (between q ~ 0.05 nm^{-1} and q ~ 0.2 nm^{-1}. This scaling is close to what is expected for elongated structures (q^{-1}). The power law at high q suggests that the interfaces are not smooth. The bump at intermediate q (q ~ 0.22 nm^{-1}) reveals a characteristic distance (28 nm) that most probably corresponds to the mean thickness of the ribbon/fiber. These results are consistent with

the morphology observed in Cryo-TEM. However, the dimensions of the self-assembled objects could not be determined from these SLS and SAXS data because they are much larger than the upper size limit of 100 nm.

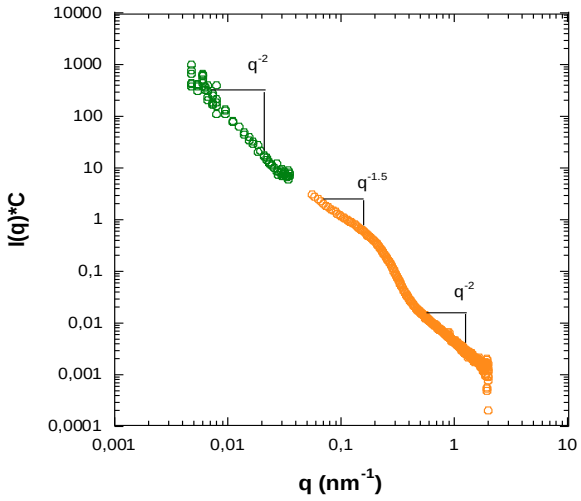

Figure 9. Combined SLS and SAXS plot obtained at 20°C for PISA suspension of P(GMA$_{65}$-*stat*-(MAm-GFF)$_7$)-*b*-PHPMA$_{28}$ diblock copolymer. The I(q) values of the y-axis were multiplied by the suitable coefficients (C) according to the dilution factors for running samples.

To explain the formation of these block copolymer structures, we surmise that the P(GMA$_{65}$-*stat*-(MAm-GFF)$_7$) macro-CTA aggregates at 70°C (the temperature of the PISA protocol here), act as an exogeneous interface for heterogeneous nucleation for the self-assembly of the diblock copolymer. Indeed, the P(GMA$_{65}$-*stat*-(MAm-GFF)$_7$)-*b*-PHPMA$_{28}$ diblock copolymer fibrous morphologies prepared *via* PISA and described above have never been reported for PGMA-*b*-PHPMA block copolymers. A PGMA$_{65}$-*b*-PHPMA$_{28}$ block copolymer would probably not self-assemble and if it did, would only lead to small spheres.[11, 74, 75] These results strongly suggests that: 1) the peculiar structures observed here are directly caused by the GFF sequences in the macro-CTA, 2) the effect of the SAP is very strong even in

polymers containing an average of only seven GFF moieties per molecule, and 3) the GFF sequences are accessible and remain active during the PISA process.

Temperature-induced morphological changes

A remarkable temperature-induced morphological change of the fiber-like structures formed from the P(GMA_{65}-*stat*-(MAm-$GFF)_7$)-*b*-$PHPMA_{28}$ block copolymer was detected by both DLS and TEM analysis. As seen in Figure **10**, upon heating from 20 °C to 70 °C, the bimodal distribution centered at 2 μm and 40 - 50 nm of the self-assembled objects was significantly modified: the peak at 2 μm decreased in intensity and shifted to 200 nm while the smaller size distribution increased in intensity. It is important to note that these changes were completely reversible as the DLS measurements carried out at 20°C before and after heating to 70°C were almost identical (Figure **10**). TEM samples were prepared at 70°C from colloïdally stable solutions incubated at 70°C for at least 1 hour. These TEM images revealed worm-like structures of roughly 25 nm in diameter (Figure **10**) instead of the flower-like fiber bundles seen at 20°C (Figure **7**). Heating not only increase the mobility of the chains but is also known to weaken or even destroy hydrogen-bonds and π-π stacking.[48, 76-78] While both interactions between GFF moieties and between GFF and water were significantly reduced at high temperature, the self-assembly of P(GMA_{65}-*stat*-(MAm-$GFF)_7$)-*b*-$PHPMA_{28}$ is mainly influenced by the PHPMA block which leads to this morphological transition. PGMA-*b*-PHPMA block copolymer particles exhibit thermo-responsive behavior with reversible morphology transition from worms to spheres upon cooling to 4°C.[79] Thus, the effect of low temperature on the GFF-containing block copolymer was also studied. After incubation for 1 h at 4°C, another clear morphological change of the self-assembled structures was observed (Figure **11**). The pure fiber phase was replaced by large spherical objects (ca. 600 nm in diameter) featuring a nanostructure composed of small spheres of roughly 25 nm. These spherical clusters were reminiscent of Mimosa. The hydrophilicity increase of the PHPMA core-forming block at low temperature[59, 79-82] likely triggered the reorganization of the P(GMA_{65}-*stat*-(MAm-$GFF)_7$)-*b*-$PHPMA_{28}$ self-assembled

morphologies, suggesting that the self-assembly process of the GFF-containing block copolymer is not only driven by the specific peptide interaction part but also by the delicate hydrophilic/hydrophobic balance for the whole system.

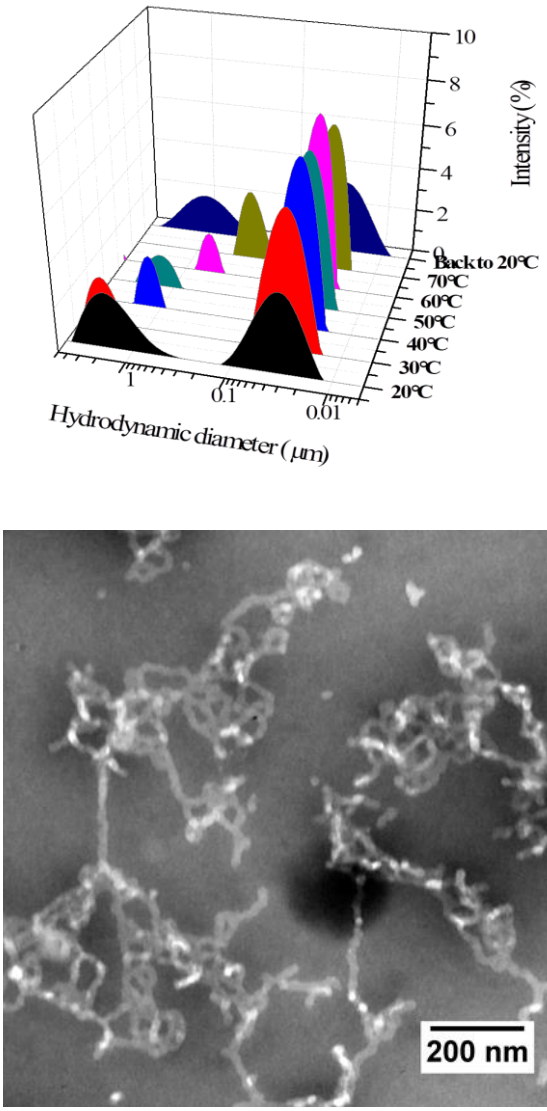

Figure 10. Evolution with temperature of the hydrodynamic diameter of P(GMA$_{65}$-*stat*-(MAm-GFF)$_7$)-*b*-PHPMA$_{28}$ diblock copolymer objects at 0.1% w/w in MilliQ water (top) and representative TEM images of P(GMA$_{65}$-*stat*-(MAm-GFF)$_7$)-*b*-PHPMA$_{28}$ block copolymer structures at 0.1% w/w in MilliQ water incubated at 70°C for 1 h (bottom).

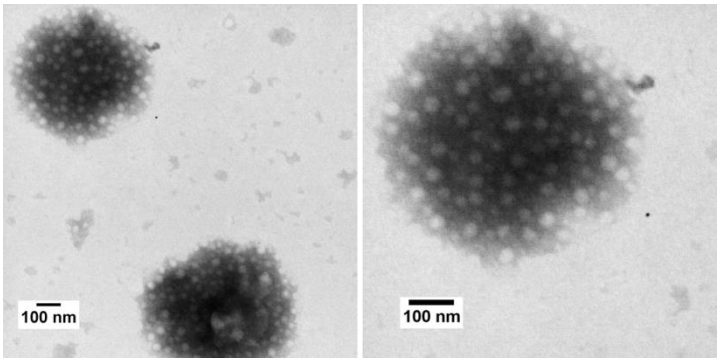

Figure 11. Representative TEM images P(GMA_{65}-*stat*-(MAm-GFF)$_7$)-*b*-$PHPMA_{28}$ block copolymer structures at 0.1% w/w in MilliQ water incubated at 4°C for 1 h.

CONCLUSIONS

RAFT aqueous dispersion polymerization protocols using GFF self-assembling peptide (SAP) were used to prepare novel nano-objects. The influence of SAP on the resulting PISA morphologies was examined. The resulting P(GMA_{65}-*stat*-(MAm-GFF)$_7$)-*b*-$PHPMA_{28}$ diblock copolymer formed self-assembled structures at 10% w/w which remained colloidally stable over six months. These structures and their evolution upon heating or cooling were examined using a combination of scattering techniques and electron microscopy. At 70°C, the highly anisotropic fibers with 1-2 µm long and 50-100 nm wide observed at 20°C were replaced by worm-like micelles. This morphological transition was fully reversible and is probably due to local rearrangement of the peptide moieties. The thermo-sensitive properties at lower temperature of PHPMA were also observed for this P(GMA_{65}-*stat*-(MAm-GFF)$_7$)-*b*-$PHPMA_{28}$ diblock copolymer morphology. After incubation at 4 °C, the rod–like structures turned into nanostructured spherical objects. This work demonstrates for the first time that the incorporation of SAP in a synthetic polymer strongly influences the shape and size of PISA-generated structures. One particularly salient point is that only seven GFF moieties per chain is sufficient to drastically change the self-assembly behavior of a diblock copolymer. This study highlights the essential role of the peptide inter-

actions in the final morphologies. Given the structural diversity of polypeptides, this paves the way for the design of a wide range of self-assembled objects that might find application as asymmetric drug delivery systems[45-47] or original scaffolds for tissue engineering for example.

ASSOCIATED CONTENT

Supporting Information

NMR spectra, HPLC profile, DDLS results.

AUTHOR INFORMATION

Corresponding Author

Mona Semsarillar - Institut Européen des Membranes, IEM, Univ Montpellier, CNRS, ENSCM, Montpellier, France, email: mona.semsarillar@umontpellier.fr

Present addresses

Thi Phuong Tuyen DAO – UPMC, Sorbonne Universités, Laboratoire PHENIX Physico-chimie des Electrolytes et Nanosystèmes Interfaciaux, CNRS, Paris, France

Email: thi-phuong-tuyen.dao@sorbonne-universite.fr

Funding Sources

PDRA fellowship managed by the French national research agency (ANR): "investissement d'Avenir" LabEX CheMISyst, grant number ANR-10-LABX-05-01. The authors also thank CNRS for funding this work via the "Osez l'interdisciplinarité" programme awarded to MS. F. Aubrit thanks M-Era.net program of Europe and the New Aquitaine Region (2017 call, FMF project) for postdoc fellowship.

REFERENCES

1. Penfold, N. J. W.; Yeow, J.; Boyer, C.; Armes, S. P., Emerging Trends in Polymerization-Induced Self-Assembly. *ACS Macro Letters* **2019,** *8*, 1029-1054.
2. D'Agosto, F.; Rieger, J.; Lansalot, M., RAFT-mediated polymerization-induced self-assembly. *Angewandte Chemie International Edition* **2020,** *59*, 8368-8392.

3. Guégain, E.; Zhu, C.; Giovanardi, E.; Nicolas, J., Radical Ring-Opening Copolymerization-Induced Self-Assembly (rROPISA). *Macromolecules* **2019,** *52*, 3612-3624.
4. Ratcliffe, L. P. D.; Ryan, A. J.; Armes, S. P., From a Water-Immiscible Monomer to Block Copolymer Nano-Objects via a One-Pot RAFT Aqueous Dispersion Polymerization Formulation. *Macromolecules* **2013,** *46*, 769-777.
5. Varlas, S.; Foster, J. C.; O'Reilly, R. K., Ring-opening metathesis polymerization-induced self-assembly (ROMPISA). *Chemical Communications* **2019,** *55*, 9066-9071.
6. Wang, J.; Wu, Z.; Wang, G.; Matyjaszewski, K., In Situ Crosslinking of Nanoparticles in Polymerization-Induced Self-Assembly via ARGET ATRP of Glycidyl Methacrylate. *Macromolecular Rapid Communications* **2019,** *40*, 1800332.
7. Darabi, A.; Jessop, P. G.; Cunningham, M. F., One-Pot Synthesis of Poly((diethylamino)ethyl methacrylate-co-styrene)-b-poly(methyl methacrylate-co-styrene) Nanoparticles via Nitroxide-Mediated Polymerization. *Macromolecules* **2015,** *48*, 1952-1958.
8. Ferguson, C. J.; Hughes, R. J.; Pham, B. T. T.; Hawkett, B. S.; Gilbert, R. G.; Serelis, A. K.; Such, C. H., Effective ab Initio Emulsion Polymerization under RAFT Control. *Macromolecules* **2002,** *35*, 9243-9245.
9. Lansalot, M.; Rieger, J., Polymerization-Induced Self-Assembly. *Macromolecular Rapid Communications* **2019,** *40*, 1800885.
10. Semsarilar, M.; Ladmiral, V.; Blanazs, A.; Armes, S. P., Anionic Polyelectrolyte-Stabilized Nanoparticles via RAFT Aqueous Dispersion Polymerization. *Langmuir* **2012,** *28*, 914-922.
11. Blanazs, A.; Madsen, J.; Battaglia, G.; Ryan, A. J.; Armes, S. P., Mechanistic Insights for Block Copolymer Morphologies: How Do Worms Form Vesicles? *Journal of the American Chemical Society* **2011,** *133*, 16581-16587.
12. Blanazs, A.; Ryan, A. J.; Armes, S. P., Predictive Phase Diagrams for RAFT Aqueous Dispersion Polymerization: Effect of Block Copolymer Composition, Molecular Weight, and Copolymer Concentration. *Macromolecules* **2012,** *45*, 5099-5107.
13. Chambon, P.; Blanazs, A.; Battaglia, G.; Armes, S. P., Facile Synthesis of Methacrylic ABC Triblock Copolymer Vesicles by RAFT Aqueous Dispersion Polymerization. *Macromolecules* **2012,** *45*, 5081-5090.
14. Semsarilar, M.; Ladmiral, V.; Blanazs, A.; Armes, S. P., Cationic Polyelectrolyte-Stabilized Nanoparticles via RAFT Aqueous Dispersion Polymerization. *Langmuir* **2013,** *29*, 7416-7424.
15. Boissé, S.; Rieger, J.; Khaled, B.; Di-Cicco, A.; Beaunier, P.; Li, M.-H.; Charleux, B., Amphiphilic block copolymer nano-fibers via RAFT-mediated polymerization in aqueous dispersed system. *Chemical communications* **2010,** *46*, 1950-1952.
16. Chaduc, I.; Crepet, A.; Boyron, O.; Charleux, B.; D'Agosto, F.; Lansalot, M., Effect of the pH on the RAFT Polymerization of Acrylic Acid in Water. Application to the Synthesis of Poly(acrylic acid)-Stabilized Polystyrene Particles by RAFT Emulsion Polymerization. *Macromolecules* **2013,** *46*, 6013-6023.
17. Zhang, W.; D'Agosto, F.; Boyron, O.; Rieger, J.; Charleux, B., One-Pot Synthesis of Poly(methacrylic acid-co-poly(ethylene oxide) methyl ether methacrylate)-b-polystyrene Amphiphilic Block Copolymers and Their Self-Assemblies in Water via RAFT-Mediated Radical Emulsion Polymerization. A Kinetic Study. *Macromolecules* **2011,** *44*, 7584-7593.
18. Chaduc, I.; Zhang, W.; Rieger, J.; Lansalot, M.; D'Agosto, F.; Charleux, B., Amphiphilic Block Copolymers from a Direct and One-pot RAFT Synthesis in Water. *Macromolecular rapid communications* **2011,** *32*, 1270-1276.
19. Derry, M.; Fielding, L.; Armes, S., Polymerization-Induced Self-Assembly of Block Copolymer Nanoparticles via RAFT Non-Aqueous Dispersion Polymerization. *Progress in Polymer Science* **2015,** *52*, 1-18.

20. Semsarilar, M.; Jones, L.; Blanazs, A.; Armes, S., Efficient Synthesis of Sterically-Stabilized Nano-Objects via RAFT Dispersion Polymerization of Benzyl Methacrylate in Alcoholic Media. *Advanced materials* **2012,** *24*, 3378-3382.
21. Jones, E. R.; Semsarilar, M.; Blanazs, A.; Armes, S. P., Efficient Synthesis of Amine-Functional Diblock Copolymer Nanoparticles via RAFT Dispersion Polymerization of Benzyl Methacrylate in Alcoholic Media. *Macromolecules* **2012,** *45*, 5091-5098.
22. Semsarilar, M.; Ladmiral, V.; Blanazs, A.; Armes, S., Poly(methacrylic acid)-based AB and ABC block copolymer nano-objects prepared via RAFT alcoholic dispersion polymerization. *Polym. Chem.* **2014,** *5*, 3466-3475.
23. Semsarilar, M.; Penfold, N.; Jones, L.; Armes, S., Semi-Crystalline Diblock Copolymer Nano-Objects Prepared via RAFT Alcoholic Dispersion Polymerization of Stearyl Methacrylate. *Polym. Chem.* **2015,** *6*, 1751-1757.
24. Zhao, W.; Gody, G.; Dong, S.; Zetterlund, P.; Perrier, S., Optimisation of the RAFT Polymerization Conditions for the in Situ Formation of Nano-objects via Dispersion Polymerization in Alcoholic Medium. *Polym. Chem.* **2014,** *5*, 6990-7003.
25. Zhang, X.; Rieger, J.; Charleux, B., Effect of the solvent composition on the morphology of nano-objects synthesized via RAFT polymerization of benzyl methacrylate in dispersed systems. *Polym. Chem.* **2012,** *3*, 1502-1509.
26. Fielding, L.; Derry, M.; Ladmiral, V.; Rosselgong, J.; Malho Rodrigues, A.; Ratcliffe, L.; Sugihara, S.; Armes, S., RAFT dispersion polymerization in non-polar solvents: Facile production of block copolymer spheres, worms and vesicles in n-alkanes. *Chem. Sci.* **2013,** *4*, 2081-2087.
27. Derry, M.; Fielding, L.; Armes, S., Industrially-Relevant Polymerization-Induced Self-Assembly Formulations in Non-Polar Solvents: RAFT Dispersion Polymerization of Benzyl Methacrylate. *Polym. Chem.* **2015,** *6*, 3054-3062.
28. Fielding, L.; Lane, J.; Derry, M.; Mykhaylyk, O.; Armes, S., Thermo-responsive Diblock Copolymer Worm Gels in Non-Polar Solvents. *Journal of the American Chemical Society* **2014,** *136*, 5790-5798.
29. Lopez-Oliva, A.; Warren, N.; Rajkumar, A.; Mykhaylyk, O.; Derry, M.; Doncom, K.; Rymaruk, M.; Armes, S., Polydimethylsiloxane-Based Diblock Copolymer Nano-objects Prepared in Nonpolar Media via RAFT-Mediated Polymerization-Induced Self-Assembly. *Macromolecules* **2015,** *48*, 3547-3555.
30. Zhang, Q.; Zhu, S., Ionic Liquids: Versatile Media for Preparation of Vesicles from Polymerization-Induced Self-Assembly. *ACS Macro Letters* **2015,** *4*, 755-758.
31. Zhou, D.; Kuchel, R. P.; Dong, S.; Lucien, F. P.; Perrier, S.; Zetterlund, P. B., Polymerization-Induced Self-Assembly under Compressed CO_2: Control of Morphology Using a CO_2-Responsive MacroRAFT Agent. *Macromolecular Rapid Communications* **2019,** *40*, 1800335.
32. Dong, S.; Zhao, W.; Lucien, F.; Perrier, S.; Zetterlund, P., Polymerization induced self-assembly: Tuning of nano-object morphology by use of CO_2. *Polym. Chem.* **2015,** *6*, 2249-2254.
33. Xu, A.; Lu, Q.; Huo, Z.; Ma, J.; Geng, B.; Azhar, U.; Zhang, L.; Zhang, S., Synthesis of fluorinated nanoparticles: Via RAFT dispersion polymerization-induced self-assembly using fluorinated macro-RAFT agents in supercritical carbon dioxide. *RSC Advances* **2017,** *7*, 51612-51620.
34. Warren, N. J.; Armes, S. P., Polymerization-Induced Self-Assembly of Block Copolymer Nano-objects via RAFT Aqueous Dispersion Polymerization. *Journal of the American Chemical Society* **2014,** *136*, 10174-10185.
35. Sugihara, S.; Blanazs, A.; Armes, S. P.; Ryan, A. J.; Lewis, A. L., Aqueous Dispersion Polymerization: A New Paradigm for in Situ Block Copolymer Self-Assembly in Concentrated Solution. *Journal of the American Chemical Society* **2011,** *133*, 15707-15713.

36. Zhang, X.; Boissé, S.; Zhang, W.; Beaunier, P.; D'Agosto, F.; Rieger, J.; Charleux, B., Well-Defined Amphiphilic Block Copolymers and Nano-objects Formed in Situ via RAFT-Mediated Aqueous Emulsion Polymerization. *Macromolecules* **2011,** *44*, 4149-4158.
37. He, W.-D.; Sun, X.-L.; Wan, W.-M.; Pan, C.-Y., Multiple Morphologies of PAA-b-PSt Assemblies throughout RAFT Dispersion Polymerization of Styrene with PAA Macro-CTA. *Macromolecules* **2011,** *44*, 3358-3365.
38. Le, D.; Keller, D.; Delaittre, G., Reactive and Functional Nanoobject(s) by Polymerization-Induced Self-Assembly. *Macromolecular Rapid Communications* **2018,** *40*, 1800551.
39. Cobo, I.; Li, M.; Sumerlin, B.; Perrier, S., Smart hybrid materials by conjugation of responsive polymers to biomacromolecules. *Nature materials* **2015,** *14*, 143-159.
40. Sumerlin, B., Proteins as Initiators of Controlled Radical Polymerization: Grafting- from via ATRP and RAFT. *ACS Macro Letters* **2012,** *1*, 141-145.
41. Li, H.; Li, M.; Yu, X.; Bapat, A.; Sumerlin, B., Block copolymer conjugates prepared by sequentially grafting from proteins via RAFT. *Polymer Chemistry* **2011,** *2*, 1531-1535.
42. Vanparijs, N.; Maji, S.; Louage, B.; Voorhaar, L.; Laplace, D.; Zhang, Q.; Shi, Y.; Hennink, W.; Richard, H.; De Geest, B., Polymer-protein conjugation via a 'grafting to' approach – A comparative study of the performance of protein-reactive RAFT chain transfer agents. *Polym. Chem.* **2015,** *6*, 5602-5614.
43. Ayres, L.; Vos, M.; Adams, P.; Shklyarevskiy, I.; Hest, J., Elastin-Based Side-Chain Polymers Synthesized by ATRP. *Macromolecules* **2003,** *36*, 5967-5973.
44. Luppi, L.; Babut, T.; Petit, E.; Rolland, M.; Quémener, D.; Soussan, L.; Semsarilar, M.; Moradi, M.-A., Antimicrobial Polylysine Decorated Nano-Structures Prepared through Polymerization Induced Self-Assembly (PISA). *Polym. Chem.* **2019,** *10*, 336-344.
45. Habibi, N.; Kamaly, N.; Memic, A.; Shafiee, H., Self-assembled peptide-based nanostructures: Smart nanomaterials toward targeted drug delivery. *Nano Today* **2016,** *11*, 41-60.
46. Webber, M. J.; Appel, E. A.; Meijer, E. W.; Langer, R., Supramolecular biomaterials. *Nature Materials* **2016,** *15*, 13-26.
47. Spicer, C.; Jumeaux, C.; Gupta, B.; M. Stevens, M., Peptide and protein nanoparticle conjugates: Versatile platforms for biomedical applications. *Chemical Society Reviews* **2018,** *47*, 3574-3620.
48. Wang, J.; Liu, K.; Xing, R.; Yan, X., Peptide self-assembly: Thermodynamics and kinetics. *Chemical Society reviews* **2016,** *45*, 5589-5604.
49. Marchesan, S.; Vargiu, A.; Styan, K., The Phe-Phe Motif for Peptide Self-Assembly in Nanomedicine. *Molecules* **2015,** *20*, 19775-19788.
50. Gazit, E., Reductionist Approach in Peptide-Based Nanotechnology. *Annual Review of Biochemistry* **2018,** *87*, 533-553.
51. Reches, M.; Gazit, E., Reches, M. & Gazit, E. Controlled patterning of aligned self-assembled peptide nanotubes. Nat. Nanotechnol. 1, 195-200. *Nature nanotechnology* **2006,** *1*, 195-200.
52. Han, T. H.; Kim, J.; Park, J. S.; Park, C.; Ihee, H.; Kim, S., Liquid Crystalline Peptide Nanowires. *Advanced Materials* **2007,** *19*, 3924-3927.
53. Yan, X.; He, Q.; Wang, K.; Duan, L.; Cui, Y.; Li, J., Transition of Cationic Dipeptide Nanotubes into Vesicles and Oligonucleotide Delivery. *Angewandte Chemie* **2007,** *46*, 2431-2434.
54. Smith, A.; Williams, R.; Tang, C.; Coppo, P.; Collins, R.; Turner, m.; Saiani, A.; Ulijn, R., Fmoc-Diphenylalanine Self Assembles to a Hydrogel via a Novel Architecture Based on π–π Interlocked β-Sheets. *Advanced Materials* **2008,** *20*, 37–41.
55. Görbitz, C., The Structure of Nanotubes Formed by Diphenylalanine, The Core Recognition Motif of Alzheimer's Beta-Amyloid Polypeptide. *Chemical communications* **2006,** *22*, 2332-2334.

56. Guo, C.; Luo, Y.; Zhou, R.; Wei, G., Probing the Self-Assembly Mechanism of Diphenylalanine-Based Peptide Nanovesicles and Nanotubes. *ACS Nano* **2012,** *6*, 3907-3918.
57. Adler-Abramovich, L.; Reches, M.; Sedman, V. L.; Allen, S.; Tendler, S. J. B.; Gazit, E., Thermal and Chemical Stability of Diphenylalanine Peptide Nanotubes: Implications for Nanotechnological Applications. *Langmuir* **2006,** *22*, 1313-1320.
58. Lovett, J. R.; Warren, N. J.; Armes, S. P.; Smallridge, M. J.; Cracknell, R. B., Order–Order Morphological Transitions for Dual Stimulus Responsive Diblock Copolymer Vesicles. *Macromolecules* **2016,** *49*, 1016-1025.
59. Warren, N. J.; Derry, M. J.; Mykhaylyk, O. O.; Lovett, J. R.; Ratcliffe, L. P. D.; Ladmiral, V.; Blanazs, A.; Fielding, L. A.; Armes, S. P., Critical Dependence of Molecular Weight on Thermoresponsive Behavior of Diblock Copolymer Worm Gels in Aqueous Solution. *Macromolecules* **2018,** *51*, 8357-8371.
60. Verber, R.; Blanazs, A.; Armes, S., Rheological studies of thermo-responsive diblock copolymer worm gels. *Soft Matter* **2012,** *8*, 9915-9922.
61. Deng, R.; Ning, Y.; Jones, L.; Cunningham, V.; Penfold, N.; Armes, S., Stimulus-responsive Block Copolymer Nano-Objects and Hydrogels via Dynamic Covalent Chemistry. *Polym. Chem.* **2017,** *8*, 5374-5380.
62. Deng, R.; Derry, M.; Mable, C.; Ning, Y.; Armes, S., Using Dynamic Covalent Chemistry To Drive Morphological Transitions: Controlled Release of Encapsulated Nanoparticles from Block Copolymer Vesicles. *Journal of the American Chemical Society* **2017,** *139*, 7616-7623.
63. C. Chan, W.; White, P. D., *Fmoc Solid-Phase Peptide Synthesis: A Practical Approach*. Oxford University Press: New York: 2000; Vol. 222.
64. Eimer, W.; Pecora, R., Rotational and translational diffusion of short rodlike molecules in solution: Oligonucleotides. *The Journal of Chemical Physics* **1991,** *94*, 2324-2329.
65. Singh, V.; Snigdha, K.; Singh, C.; Sinha, N.; Thakur, A., Understanding the self-assembly of Fmoc-phenylalanine to hydrogel formation. *Soft Matter* **2015,** *11*, 5353-5364.
66. Li, Q.; Jia, Y.; Dai, L.; Li, J., Controlled Rod Nanostructured Assembly of Diphenylalanine and Their Optical Waveguide Properties. *ACS nano* **2015,** *9*, 2689-2695.
67. Görbitz, C., Nanotube Formation by Hydrophobic Dipeptides. *Chemistry* **2002,** *7*, 5153-5159.
68. Huang, R.; Qi, W.; Su, R.; Zhao, J.; He, Z., Solvent and surface controlled self-assembly of diphenylalanine peptide: From microtubes to nanofibers. *Soft Matter* **2011,** *7*, 6418-6421.
69. Tomar, D.; Chaudhary, S.; Jena, K. C., Self-assembly of l-phenylalanine amino acid: electrostatic induced hindrance of fibril formation. *RSC advances* **2019,** *9*, 12596-12605.
70. Hatton, F.; Lovett, J.; Armes, S., Synthesis of well-defined epoxy-functional spherical nanoparticles by RAFT aqueous emulsion polymerization. *Polym. Chem.* **2017,** *8*, 4856-4868.
71. Canning, S. L.; Smith, G. N.; Armes, S. P., A Critical Appraisal of RAFT-Mediated Polymerization-Induced Self-Assembly. *Macromolecules* **2016,** *49*, 1985-2001.
72. Cunningham, V.; Alswieleh, A.; Thompson, K.; Williams, M.; Leggett, G.; Armes, S.; Musa, O., Poly(glycerol monomethacrylate)–Poly(benzyl methacrylate) Diblock Copolymer Nanoparticles via RAFT Emulsion Polymerization: Synthesis, Characterization, and Interfacial Activity. *Macromolecules* **2014,** *47*, 5613-5623.
73. Ladmiral, V.; Semsarilar, M.; Canton, I.; Armes, S. P., Polymerization-Induced Self-Assembly of Galactose-Functionalized Biocompatible Diblock Copolymers for Intracellular Delivery. *Journal of the American Chemical Society* **2013,** *135* (36), 13574-13581.
74. Mable, C. J.; Thompson, K. L.; Derry, M. J.; Mykhaylyk, O. O.; Binks, B. P.; Armes, S. P., ABC Triblock Copolymer Worms: Synthesis, Characterization, and Evaluation as Pickering Emulsifiers for Millimeter-Sized Droplets. *Macromolecules* **2016,** *49*, 7897-7907.

75. Li, Y.; Armes, S., RAFT Synthesis of Sterically Stabilized Methacrylic Nanolatexes and Vesicles by Aqueous Dispersion Polymerization. **2010,** *49*, 4042-4046.
76. Huang, R.; Wang, Y.; Qi, W.; Su, R.; He, Z., Temperature-induced reversible self-assembly of diphenylalanine peptide and the structural transition from organogel to crystalline nanowires. *Nanoscale research letters* **2014,** *9*, 653.
77. Kim, J.; Han, T. H.; Kim, Y.-I.; Park, J. S.; Choi, J.; Churchill, D.; Kim, S.; Ihee, H., Role of Water in Directing Diphenylalanine Assembly into Nanotubes and Nanowires. *Advanced materials* **2010,** *22*, 583-587.
78. Yang, D.; Gao, S.; Fang, Y.; Lin, X.; Jin, X.; Wang, X.; Ke, L.; Shi, K., The π–π stacking-guided supramolecular self-assembly of nanomedicine for effective delivery of antineoplastic therapies. *Nanomedicine* **2018,** *13* (24), 3159-3177.
79. Blanazs, A.; Verber, R.; Mykhaylyk, O. O.; Ryan, A. J.; Heath, J. Z.; Douglas, C. W. I.; Armes, S. P., Sterilizable Gels from Thermoresponsive Block Copolymer Worms. *Journal of the American Chemical Society* **2012,** *134*, 9741-9748.
80. Ratcliffe, L.; Derry, M.; Ianiro, A.; Tuinier, R.; Armes, S., A Single Thermoresponsive Diblock Copolymer Can Form Spheres, Worms or Vesicles in Aqueous Solution. *Angewandte Chemie International Edition* **2019,** *58*, 18964-18970.
81. North, S. M.; Armes, S. P., Aqueous solution behavior of stimulus-responsive poly(methacrylic acid)-poly(2-hydroxypropyl methacrylate) diblock copolymer nanoparticles. *Polymer Chemistry* **2020,** *11*, 2147-2156.
82. Penfold, N. J. W.; Whatley, J. R.; Armes, S. P., Thermoreversible Block Copolymer Worm Gels Using Binary Mixtures of PEG Stabilizer Blocks. *Macromolecules* **2019,** *52*, 1653-1662.